Si^+ ion implantation for strain relaxation of pseudomorphic $Si_{1-x}Ge_x/Si(100)$ heterostructures

D. Buca, R. A. Minamisawa, H. Trinkaus, B. Holländer, S. Mantl, R. Loo, and M. Caymax

Citation: Journal of Applied Physics **105**, 114905 (2009);
View online: https://doi.org/10.1063/1.3139274
View Table of Contents: http://aip.scitation.org/toc/jap/105/11
Published by the American Institute of Physics

Si^+ ion implantation for strain relaxation of pseudomorphic $Si_{1-x}Ge_x/Si(100)$ heterostructures

D. Buca,[1,a] R. A. Minamisawa,[1] H. Trinkaus,[1] B. Holländer,[1] S. Mantl,[1] R. Loo,[2] and M. Caymax[2]
[1]*Institute of Bio- and Nanosystems (IBN1-IT), Forschungszentrum Jülich, D-52425 Jülich, Germany and JARA-Fundamentals of Future Information Technology*
[2]*IMEC, Kapeldreef 75, B-3001 Leuven, Belgium*

(Received 21 November 2008; accepted 25 April 2009; published online 3 June 2009)

A mechanism of strain relief of pseudomorphic $Si_{1-x}Ge_x/Si(100)$ heterostructures by Si^+ ion implantation and annealing is proposed and analytically modeled. The degree of strain relaxation is presented as a function of Ge content and implantation and annealing parameters. Rutherford backscattering spectrometry/channeling, Raman spectroscopy, and transmission electron microscopy are employed to quantify the efficiency of the relaxation process and to examine the quality of the samples, respectively. The mechanism and the conditions for strain relaxation are discussed in terms of dislocation loop formation in the implanted range with emphasis on loop formation in the compressively strained SiGe layer. The detrimental effect of local amorphization of the SiGe layer on its relaxation and on strain transfer to the Si-cap layer is also addressed. © *2009 American Institute of Physics*. [DOI: 10.1063/1.3139274]

I. INTRODUCTION

Strained silicon (sSi) technology has emerged as a powerful technique for efficiently increasing the carrier mobility and the drive current in complementary metal oxide semiconductor field effect transistors (CMOS-FETs).[1] Substrate engineering such as combining sSi and silicon on insulator (SOI) technologies[2,3] made it possible to improve the IC performance by increasing the drive current and reducing leakage and power consumption.[4] Two types of substrates at wafer level are evaluated by the IC industry: sSi directly on insulator[2,4] and strained silicon on relaxed silicon germanium on insulator.[5] For both approaches high quality strain-relaxed SiGe layers grown on a Si substrate are required as virtual substrates.[6,7]

There are several reports regarding the relaxation of strained SiGe grown on Si (100) by ion implantation. Detailed studies of efficient stress relaxation of SiGe layers by the implantation of light ions such as H^+ or He^+ and subsequent annealing were published.[8–10] It was shown that under such conditions, cavities filled with gas under extremely high pressure emit dislocation loops, which glide to the Si/SiGe interface where they form strain relaxing misfit segments.[11]

The implantation of heavier ions into Si followed by annealing is known to result in the formation of defect clusters such as {311} defects,[12,13] as well as faulted and perfect dislocation loops.[14–16] Regarding Si ion implantation, intensive studies were dedicated to the thermal evolution of such induced defects and to their changes from one crystallographic structure to another.[13,14] Most of this defect research was related to transient enhanced diffusion of dopants such as B or P, ultrashallow junction, and leakage junction control via extended defect structures.

Holländer *et al.* proposed Si^+ ion implantation into the Si substrate followed by annealing for the purpose of strain relaxation of pseudomorphic SiGe layer grown on SOI material.[17] In the case of He, interstitial type dislocation loops are formed upon pressure relaxation of He filled cavities during annealing, while in the case of Si implantation, dislocation loops form due to the clustering of excess self-interstitial atoms (SIAs) corresponding to the implanted Si ions. The reported experiment was primarily aimed at demonstrating the potential of Si^+ implantation for strained SiGe layer relaxation. Its preliminary success suggests a systematic study to elucidate in particular dislocation loop formation within SiGe layers and their contribution to strain relaxation.

Therefore, the goal of the present work was to study the mechanism of strain relaxation of SiGe layers by Si ion implantation and annealing. To this end, a series of Rutherford backscattering spectrometry/channeling (RBS/C), Raman spectroscopy, and transmission electron microscopy (TEM) experiments were carried out to investigate the dependence of the relaxation degree of SiGe layers with different Ge contents on implantation energy and ion dose.

Our experimental results reveal a high sensitivity of the relaxation degree of SiGe layers and of the quality of the heterostructures with respect to the ion implantation dose. These findings are modeled in terms of formation and growth of dislocation loops in *strained SiGe layer* and their transformation into strain relieving threading dislocations (TDs) and misfit segments spreading over the SiGe layer. The dislocation driven strain transfer mechanism between the SiGe layer and the Si-cap layer, first observed for the case of SiGe layer relaxation using He^+ ion implantation and annealing,[10] is studied as a function of the Si implantation dose.

The disturbance of the described mechanisms and the detrimental effects of temporary local amorphization of the SiGe layer on these processes and on the quality of the struc-

[a]Electronic mail: d.m.buca@fz-juelich.de.

tures are discussed. In summary we devote this article to the concept of Si ion implantation for SiGe strain relaxation, which is not only restricted to our specific experimental conditions but contributes to a more general understanding of strained layer relaxation.

II. EXPERIMENTAL

Pseudomorphic Si-cap/SiGe layers were grown on 200 mm Si(100) wafers by chemical vapor deposition in a production ASM Epsilon reactor. The SiGe layer thickness h_{SiGe} was kept below the metastable critical thickness for pseudomorphic growth on Si substrate depending on the Ge content as follows: 180 nm $Si_{0.8}Ge_{0.2}$, 150 nm $Si_{0.74}Ge_{0.26}$, and 140 nm $Si_{0.71}Ge_{0.29}$. We kept the thickness of the Si-cap layer as thin as 6 nm in order not to hamper SiGe relaxation. Furthermore, the chosen layer stack allows a simultaneous relaxation of the SiGe layer and strain buildup in the Si-cap layer, as further discussed in Sec. III D. Since we cannot necessarily assume that the optimal implantation depth is the same as for H^+ or He^+ ion implantation (into the Si substrate adjacent to the SiGe/Si interface), we examined and compared the effects of Si^+ implantation into the SiGe layer at the SiGe/Si interface as well as into the Si substrate. Consequently, Si^+ ions were implanted at room temperature with different energies chosen such that the medium ion projected ranges (R_p) correspond to certain selected distances from the SiGe/Si interface, $D=R_p-h_{SiGe}$. For the relation between Si^+ implantation energy and the implanted Si distribution, the simulation software SRIM2008 was used.[18] Figure 1 shows, as examples, the results of simulations of 55 and 180 keV Si^+ ion implantation into 150 nm thick $Si_{0.74}Ge_{0.26}/Si(100)$. In Figs. 1(a) and 1(b) the Si ion and vacancy distribution profiles are shown, respectively. The Si^+ ion implantation dose (fluence) is tuned between a lower limit of 4×10^{13} ions/cm^2 defined by a small strain relaxation effect and an upper limit of 1.5×10^{14} ions/cm^2 characterized by substantial amorphization. In Table I, the implantation energies and doses considered for three combinations of Ge content and thicknesses of the SiGe layers are listed. After implantation, the wafers were annealed in inert atmosphere by standard rapid thermal processing (RTP) at different temperatures.

We present a systematic analysis of crystalline quality of the SiGe layer during the relaxation process using RBS/C. The degree of crystallinity is evaluated by the minimum yield of backscattered He^+ ions below the surface peak signal defined as the ratio of the intensity of the random and aligned spectra. A detailed description of this technique was reported by Feldman *et al.*[19] The Ge atomic fraction was determined by simulating the RBS spectra using the RUMP code.[20] RBS/C measurements were performed using a Tandetron accelerator with 1.4 MeV He^+ ions using a backscattered angle of 170°.

The elastic strain in the $Si_{1-x}Ge_x$ epilayers was measured by Raman spectroscopy using a wavelength of 480 nm and restricted to low laser-power density in order to avoid thermal strain relaxation. For detailed information on the layer morphology the sample was characterized by TEM and plane-view TEM using a JEOL 4000 FX microscope.

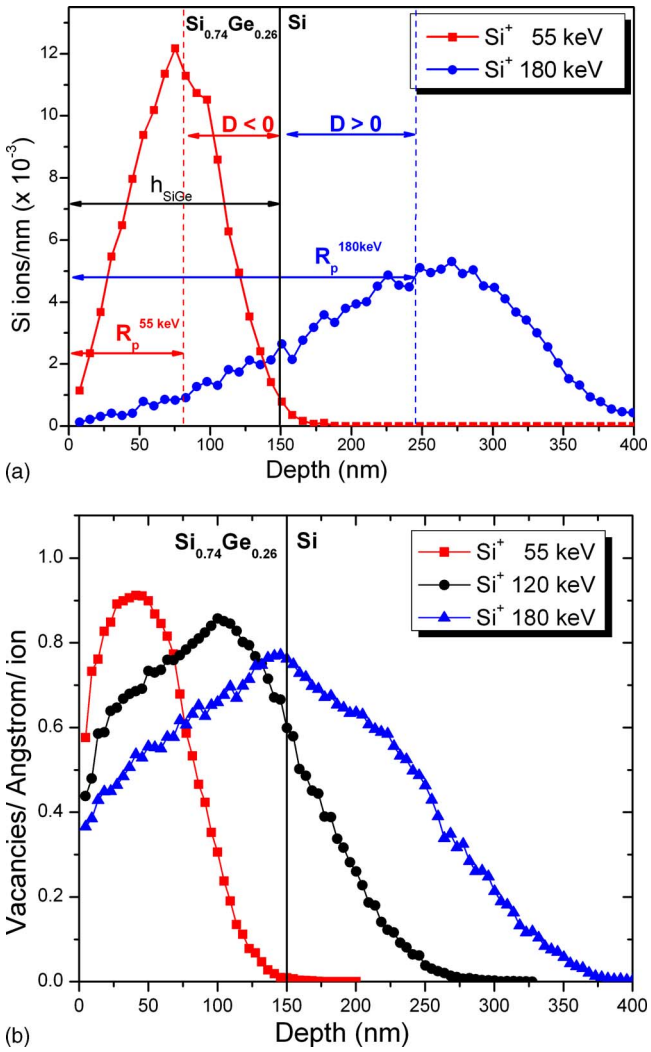

FIG. 1. (Color online) Profiles of (a) Si^+ ion distribution and (b) vacancy distribution in a 150 nm $Si_{0.74}Ge_{0.26}$ layer for implantation energies of 55 keV ($D<0$) and 180 keV ($D>0$), where D is the medium ion projected range measured from the SiGe/Si interface.

III. RESULTS

In order to establish a systematic sequence for the experiments and discussions, three different situations regarding the implantation depth are first discussed: in Sec. III A, Si ion implantation into the epitaxial SiGe layer ($D<0$); in Sec. III B, Si ion implantation at the SiGe/Si(100) interface ($D=0$); and in Sec. III C Si ion implantation into the substrate ($D>0$). In the subsequent Sec. III D, these situations are analyzed with respect to the strain induced into the Si-cap layer during SiGe layer relaxation. Section III E summarizes the influence of the Ge content on the Si ion implantation dose required for an efficient relaxation process.

A. Silicon implantation into the SiGe layer ($D<0$)

Figure 2 shows the RBS/C spectra of 150 nm $Si_{0.74}Ge_{0.26}$ layers, strain relaxed by 55 keV Si^+ ion implantation ($D\sim-70$ nm) at different doses followed by an 850 °C, 600 s anneal. The lowest applied implantation dose of 5×10^{13} ions/cm^2 yields an insufficient relaxation degree of only $R=49\%$ and a low crystal quality characterized by a

TABLE I. List of Ge content and thickness of SiGe layers considered, together with implantation parameters (energies and doses) applied.

Ge content (%)	SiGe layer thickness (nm)	Energy (keV)	Implanted Si dose (ions/cm^2)
20	180	195	1.0×10^{14}
			1.5×10^{14}
26	150	55	5.0×10^{13}
			8.5×10^{13}
			1.0×10^{14}
			1.5×10^{14}
		120	4.0×10^{13}
			7.0×10^{13}
			8.5×10^{13}
			1.0×10^{14}
			1.15×10^{14}
		180	8.5×10^{13}
			1.0×10^{14}
			1.5×10^{14}
29	140	110	8.5×10^{13}
			1.0×10^{14}
		180	8.5×10^{13}
			1.0×10^{14}

channeling minimum yield of $\chi_{min}=6.2\%$, which is significantly higher than the value of $\chi_{min}=4\%$ for the as-grown sample (black solid line). Implantation of 1×10^{14} ions/cm^2 results in an acceptable relaxation ($R=77\%$) with a similarly low layer quality ($\chi_{min}=6.4\%$). At the highest applied dose of 1.5×10^{14} at/cm^2, the SiGe layer is heavily damaged. Annealing at 850 °C for 10 min results in a recovery of its crystallinity, even though only to $\chi_{min}=9.8\%$, and very efficient relaxation ($R=92\%$), however, useless for applications that require layers with $\chi_{min}<5\%$. Hence, independently of the implantation fluence, at negative D values, the layer quality is always low. This observation is confirmed by TEM images showing residual dislocations loops (typically of interstitial type) in all the analyzed samples, as exemplified in Fig. 3.

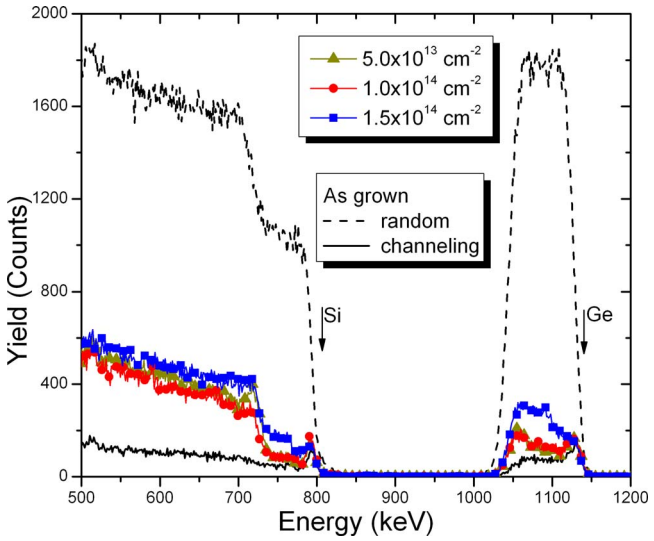

FIG. 2. (Color online) Channeling spectra of the 150 nm thick $Si_{0.74}Ge_{0.26}$ implanted with 55 keV Si$^+$ ions to 5×10^{13} ions/cm^2 (full green triangle line), 1×10^{14} ions/cm^2 (full red circle line), and 1.5×10^{14} ions/cm^2 (full blue square line) and postannealed at a temperature of 850 °C for 600 s. The random (black dashed line) and channeling (black full line) spectra of the as grown sample are shown for reference.

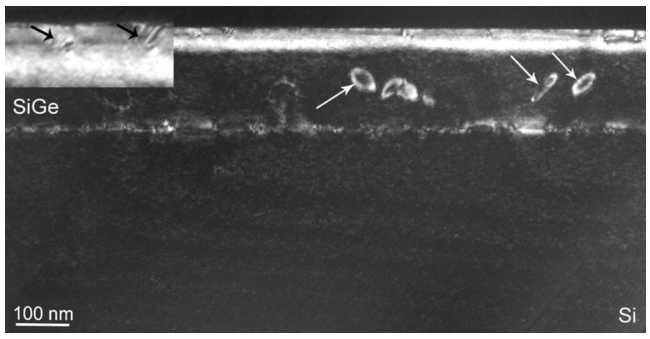

FIG. 3. Dark field XTEM image of the 150 nm thick $Si_{0.74}Ge_{0.26}$ after 55 keV ($D\sim-70$) Si$^+$ implantation to 1×10^{14} ions/cm^2 and 850 °C annealing for 600 s. Residual dislocation loops formed in the SiGe layer are marked by white arrows, while the black arrows indicate TD arms blocked in the Si-cap layer. Defects in the Si-cap layer and at the Si-cap/SiGe interface are considered to be responsible for the loss in the strain transfer documented in Table II.

B. Silicon implantation centered at the SiGe/Si(100)interface ($D\sim0$)

Implantation close to the SiGe/Si(100) interfaces induces defect areas at both sides of the interface. In this case one could imagine that loops are formed in the substrate and glide to the close-by interface, similar to the case of H$^+$/He$^+$ implantation,[11] and that the extension of the loops through the SiGe layer would be supported by the defects there.

In Fig. 4, [100] channeling spectra of 150 nm thick $Si_{0.74}Ge_{0.26}$ implanted with 120 keV Si$^+$ ions and annealed at 850 °C for 600 s are compared with those of unimplanted samples. At this implantation energy, D is approximately zero and the implantation indeed induces defect regions at both sides of the SiGe/Si(100) interface as intended. The lowest applied implantation dose of 4×10^{13} ions/cm^2

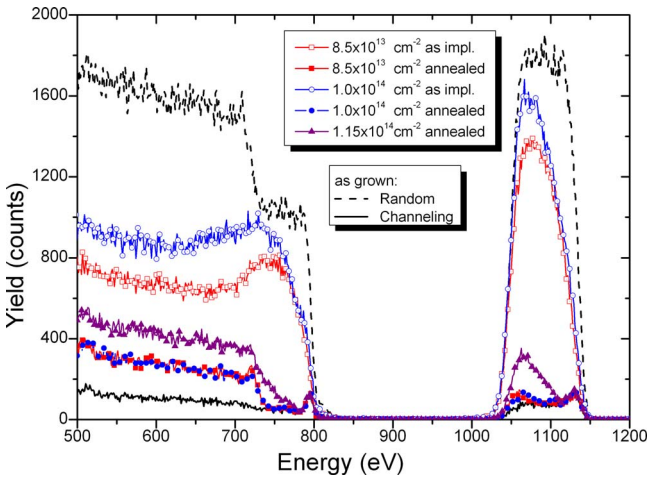

FIG. 4. (Color online) Channeling spectra of the 150 nm thick $Si_{0.74}Ge_{0.26}$ implanted with 120 keV Si$^+$ ions to 8.5×10^{13} ions/cm^2 (red), 1×10^{14} ions/cm^2 (blue), and 1.15×10^{14} ions/cm^2 (violet) for the as-implanted (empty symbols) and postannealed at 850 °C for 600 s (full symbols). The random (black dashed line) and channeling (black line) spectra of the as grown sample are shown for reference.

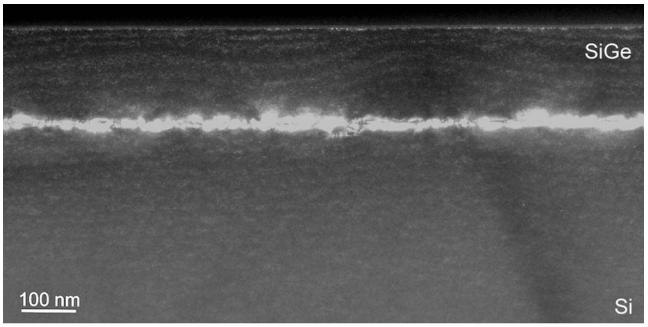

(a)

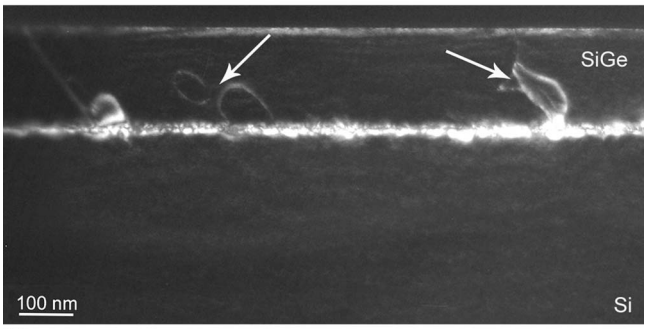

(b)

FIG. 5. XTEM image of the 150 nm thick $Si_{0.74}Ge_{0.26}$ after 120 keV Si^+ implantation ($D \sim 0$) at (a) 8.5×10^{13} and (b) 1×10^{14} ions/cm^2 and annealing at 850 °C for 600 s. In (b) residual dislocation loops in the SiGe layer (marked by white arrows) not efficient in the relaxation process are observed.

yields virtually no contribution to the relaxation of the strained SiGe layer. An increase in the dose to 7×10^{13} ions/cm^2 increases the relaxation to a still insufficient value of only $R=47\%$. Further increase in the fluence to 8.5×10^{13} and 1×10^{14} ions/cm^2 (square and circle lines) increases strain relaxation to $R=77\%$ at high quality characterized by low minimum yields of $\chi_{min}=4.2\%$ and $\chi_{min}=4.4\%$, respectively. For an even higher implantation fluence of 1.15×10^{14} ions/cm^2, the SiGe layer is relaxed by $R=73\%$ but has a low layer quality characterized by $\chi_{min}=6\%$ (up-triangle line). This dose dependence of the relaxation degree reveals a very strong dose sensitivity of the relaxation process, which has not been observed for SiGe relaxation by He^+/H^+ implantations.[21]

The dark field cross-sectional TEM (XTEM) images of 150 nm thick $Si_{0.74}Ge_{0.26}$ samples implanted at $D \sim 0$, presented in Fig. 5, show strong contrast at the SiGe/Si interface, indicating the formation of misfit dislocations (MDs). For an implantation of 8.5×10^{13} ions/cm^2 [Fig. 5(a)] no residual dislocation loops are observed in the SiGe layer. In contrast to this, at 1×10^{14} ions/cm^2, residual loops pinned in the SiGe layer can be seen in Fig. 5(b), confirming that relaxation is indeed associated with dislocation loops. No {311} defects were observed in the SiGe layers, suggesting that dislocation loops form there directly by self-interstitials condensation during annealing, i.e., without {311} defects as intermediate defects.[15]

The TD density measured by plane-view TEM showed the lowest values of $3-4 \times 10^7$/cm^2 for Si implantation of 8.5×10^{13} ions/cm^2. This TD density is higher than the one

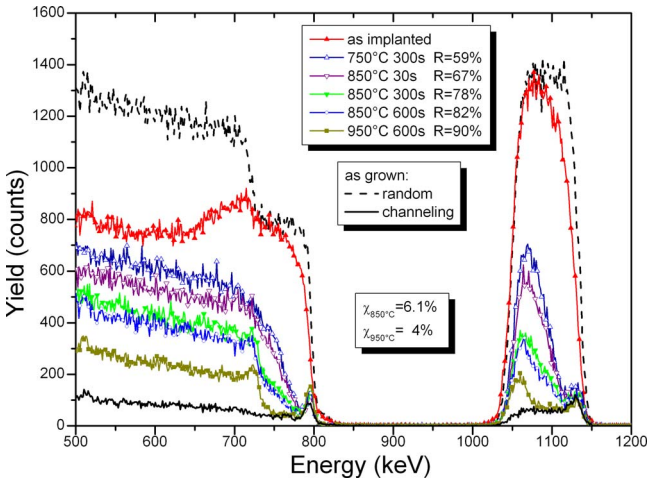

FIG. 6. (Color online) Channeling spectra of 150 nm $Si_{0.74}Ge_{0.26}$ layers after 180 keV 1.5×10^{14} Si^+/cm^2 implantation and different RTP annealing temperatures. The random (black dashed line) and channeling (black solid line) spectra of the as grown sample are shown for reference. In the legend, the minimum yield and the layer relaxation degree are given for every annealing condition.

obtained using He^+ ion implantation where for an optimized process values of 6×10^5/cm^2 are measured.[2,9]

C. Silicon implantation into the substrate ($D>0$)

Following the same strategy as in the Secs. III A and III B, Si^+ ions were implanted with a high energy of 180 keV into Si below 150 nm thick $Si_{0.74}Ge_{0.26}$ layers ($D \sim 80$ nm). The implantation dose was chosen such that a sufficiently high density of {311} defects is produced in Si, assuming that this would result in a sufficiently high density of dislocation loops active for strain relaxation.

At this implantation energy of 180 keV, the dose of 8.5×10^{13} ions/cm^2, which gives the best result for 120 keV implantation, yields only insignificant relaxation of 35%. Increase in the dose to 1×10^{14} ions/cm^2, where the top of SiGe layer still remains crystalline during implantation, results in a steep increase in relaxation degree to 78%. The low channeling minimum yield $\chi_{min}=4.1\%$ indicates a high crystalline layer quality for this dose. Further increase in the dose to 1.5×10^{14} Si^+/cm^2 is associated with amorphization during implantation as shown in Fig. 6 where the channeling spectrum after implantation approaches the random spectrum of the as grown sample for part of the layer.

Figure 6 compares the RBS/C spectra of a 150 nm $Si_{0.74}Ge_{0.26}$ layers at different annealing states during the recrystallization process. After 750 °C annealing for 300 s, the lower part of the SiGe layer is severely damaged. This is also confirmed by the XTEM micrograph in Fig. 7(a) where, in addition, the formation of {311} defects in the Si substrate is observed. The SiGe layer recovers its crystallinity with increasing annealing temperature and time. After 850 °C RTP annealing for 600 s the layer is fully recrystallized and relaxed by 80%. However, the channeling minimum yield of $\chi_{min}=6\%$ indicates a low crystalline quality, in agreement with the high defect density observed in the XTEM micrograph shown in Fig. 7(b). Moreover, Fig. 7(b) proves the loops formation in the SiGe layer and the conversion {311}

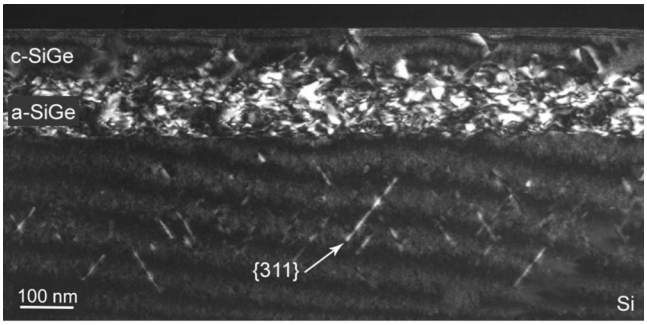

(a)

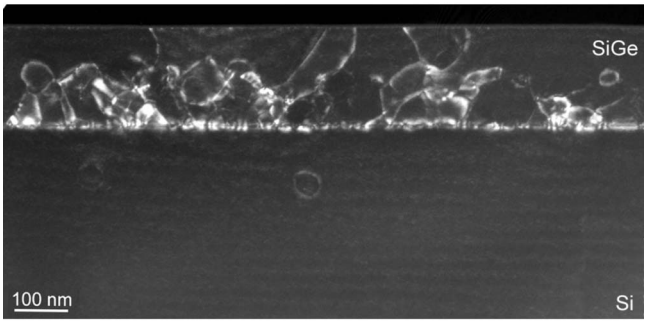

(b)

FIG. 7. (a) XTEM image of the 150 nm thick $Si_{0.74}Ge_{0.26}$ after 180 keV Si^+ implantation at 1.5×10^{14} ions/cm^2 and RTP annealing at 700 °C for 300 s indicating the amorphized region of the SiGe layer and the {311} defects formed in the Si substrate. (b) XTEM image of the 150 nm thick $Si_{0.74}Ge_{0.26}$ after 180 keV Si^+ implantation at 1.5×10^{14} ions/cm^2 and RTP annealing at 850 °C for 600 s. The arrows point to the dislocations loops formed in the SiGe layer and Si substrate.

defects in the substrate into dislocation loops [see Fig. 7(a)]. Annealing at 950 °C reduces the channeling yield to a minimum of 4% and results in 88% relaxation of the SiGe layer. However, recrystallization induced layer relaxation and Ge out-diffusion into Si cap occurring at such high temperatures is undesirable. In the case of 850 °C annealing the maximum Ge interdiffusion into Si cap is about 1–2 nm.

The results obtained for the strain relaxation and quality of a 150 nm thick $Si_{0.74}Ge_{0.26}$ layers are summarized in the Table II. For the doses considered, the relaxation degree and the channeling minimum yield are plotted in Fig. 8 versus the implanted ion range [Figs. 8(a) and 8(c)] and Si implantation dose [Figs. 8(b) and 8(d)]. The marked areas indicate the implantation parameter sets for which either efficient relaxation (>70%) or good layer quality ($\chi_{min}<5\%$) is obtained. In the next section, we will discuss the values listed in Table II for the measured strain in the Si cap.

D. Strain transfer to Si-cap layers

Thin Si layer capping is preferred during SiGe material processing. It allows standard Si cleaning processes and reduces SiGe surface roughness during thermal annealing, and it can serve as seed layer for optional epitaxial overgrowth. For nanoelectronic applications, such a thin Si layer subjected to strain by strain transfer as described below and transferred on a second oxidized wafer is sufficient for the realization of ultrathin SOI MOSFETs.[22]

Strain buildup in Si-cap layers during strain relaxation of adjacent SiGe layers was studied as a function of Si-cap thickness for the case of He^+ ion implantation and annealing.[10] Full strain transfer from the relaxing SiGe layer to the Si-cap layer was found up to a critical Si layer thickness of 8 nm. The SiGe layers discussed in this paper are covered by 6 nm thick Si-cap layers, which are, therefore, expected to accept the full strain corresponding to the strain change in the relaxing SiGe layers. In the following we study the strain transfer mechanism as a function of the Si ion implantation dose. To quantify the efficiency of the strain transfer, we have defined in Ref. 10 the ratio of the strain induced in the Si top layer to the strain change in the SiGe layer as the strain transfer efficiency η.

From Raman spectroscopy, both the relaxation of the SiGe and the strain induced in the Si-cap layer and hence the strain transfer efficiency can be deduced.[23] In Fig. 9, Raman spectra for 150 nm thick $Si_{0.74}Ge_{0.26}$ implanted with 180 keV Si^+ to three different doses are presented. The shift in the small peak corresponding to Si vibration modes in the Si-cap

TABLE II. Degree of relaxation, channeling minimum yield, maximum possible strain and measured strain in the Si top layer, strain transfer efficiency for 150 nm thick $Si_{0.74}Ge_{0.26}$ as a function of Si ion energy, and dose. The RTP annealing parameters for all cases were 850 °C for 600 s.

Energy (keV)	Si implantation dose (ions/cm^2)	SiGe relaxation degree (%)	Minimum channeling yield (%)	Max. strain in Si cap (%)	Measured strain in Si cap (%)	Strain transf. efficiency (%)
55	5.0×10^{13}	49	6.2	0.53	0.50	94
	8.5×10^{13}	79	[a]	0.86	0.65	76
	1.0×10^{14}	77	6.4	0.84	0.64	76
	1.5×10^{14}	92	9.8	1.00	0	0
120	4.0×10^{13}	10	[a]	0.10	0.10	100
	7.0×10^{13}	47	5.1	0.51	0.5	98
	8.5×10^{13}	77	4.2	0.84	0.80	95
	1.0×10^{14}	77	4.4	0.84	0.71	86
	1.15×10^{14}	73	6	0.79	0.52	67
180	8.5×10^{13}	35	[a]	0.40	0.40	100
	1.0×10^{14}	78	4.1	0.85	0.72	85
	1.5×10^{14}	82	6.1	0.90	0	0

[a]Not measured.

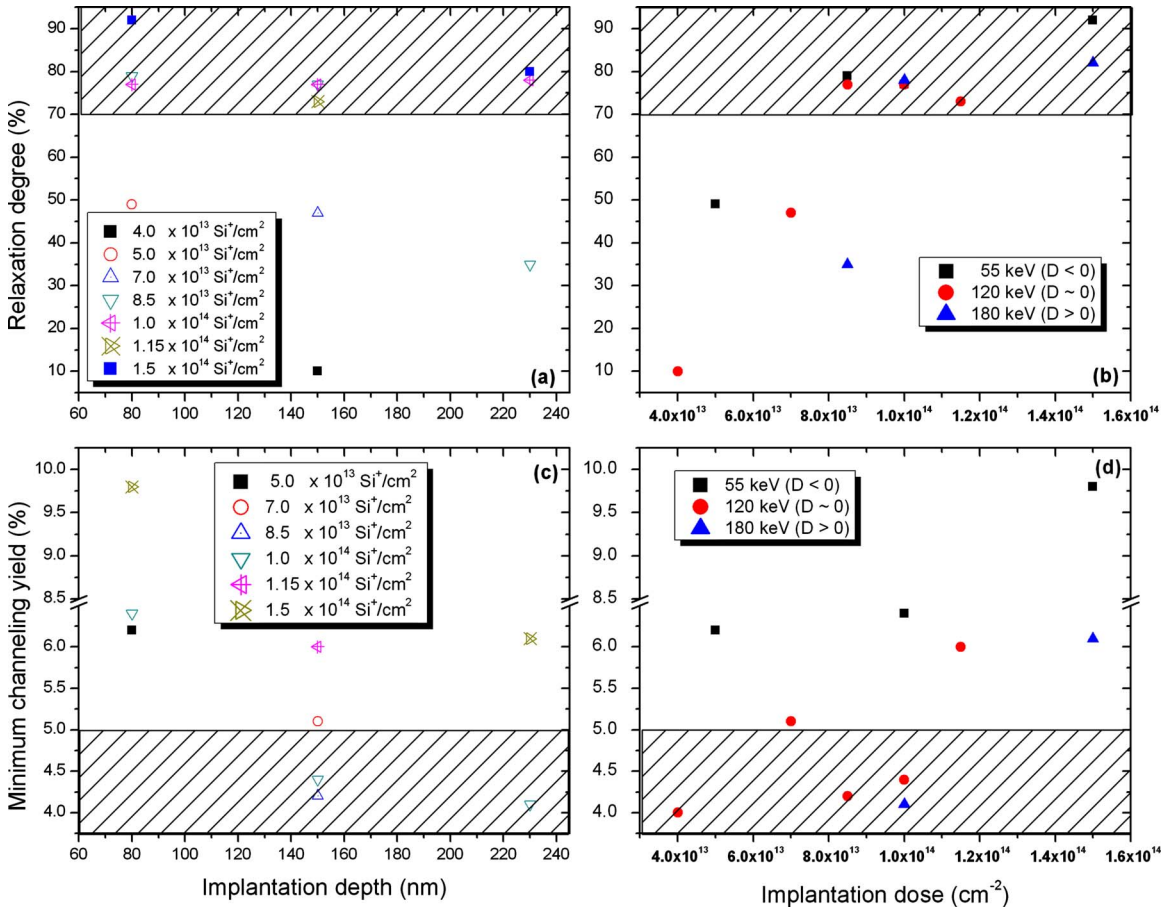

FIG. 8. (Color online) Representation of the relaxation degree of the SiGe layer and the channeling minimum yield vs the implanted ion range [(a) and (c)] and vs Si ion implantation dose [(b) and (d)] for the parameters considered in the paper.

layer reveals the tensile strain status in the film. For a SiGe relaxation using a low Si ion implantation dose of 8.5×10^{13} ions/cm^2, the SiGe degree of relaxation of only 35% induces a strain in the Si cap of $\varepsilon = 0.40\%$ corresponding to a transfer efficiency of $\eta = 100\%$. Using a higher Si implantation dose of 1.0×10^{14} Si$^+$/cm^2 the SiGe relaxation increases to 78% but the strain in Si cap only to $\varepsilon = 0.72\%$, corresponding to $\eta = 85\%$. According to the dislocation dynamics model presented in Ref. 10, part of the spreading TD arms relaxing the SiGe layer cannot overcome the SiGe/Si interface where they form MDs (details will be given in the discussion section). Figure 3 shows the result of a 55 keV Si$^+$ implantation to 1×10^{14} ions/cm^2 with some TD arms blocked in the Si cap. In the case of a 180 keV Si$^+$ implantation to a high dose of 1.5×10^{14} ions/cm^2, where substantial amorphization/recrystallization occurs, no strain induced in the Si cap can be measured (for explanation see Sec. IV B).

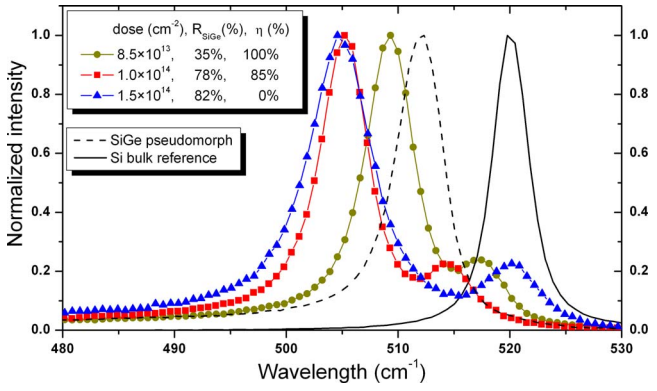

FIG. 9. (Color online) Raman spectra of Si–Si modes from SiGe and Si-cap epitaxial films of a $Si/Si_{0.74}Ge_{0.26}/Si$ (100) heterostructures after 180 keV Si$^+$ implantation and different strain relaxation procedures. The pseudomorph SiGe grown and bulk Si spectrum are shown for comparison.

Also the widths of the Raman peaks provide information on the quality of the strain relaxation process. The deconvolution of the sSi and SiGe signals does not result in significant change in the width of the Raman peaks for the first two implantation doses, indicating a uniform strain distribution in the SiGe and sSi layers. For the high dose inducing amorphization, both Raman peaks show considerable broadening. We interpret this as the result of high stress variations in the SiGe layer and of low quality of both materials.

The same analysis was applied to all other cases ($D < 0$ and $D \sim 0$) discussed in this paper. The experimentally measured strains in the Si cap and the maximum possible strains corresponding to the relaxation of the SiGe layers are presented in Table II. We conclude that using Si ion implantation, 100% strain transfer is obtained only for the cases with insufficient strain relaxation. For a very limited parameter window, relaxed SiGe layers useful for application are obtained with a reasonable strain transfer of over 85%.

TABLE III. List of SiGe layers (implantation depth, germanium content, layer thickness, and dose) that yield the best results (relaxation degree and quality).

	Germanium content (at. %)	SiGe layer thickness (nm)	Si implantation dose (ions/cm^2)	SiGe relaxation degree (%)
$D \gg 0$	20	180	1.5×10^{14}	74
	26	150	1.0×10^{14}	77
	29	140	8.5×10^{13}	80
$D=0$	26	150	8.5×10^{13}	77
	29	140	8.5×10^{13}	78

E. Influence of the germanium content on the SiGe relaxation

In the present subsection the relaxation parameters are presented as a function of the Ge content in the SiGe alloy. We will limit ourselves to the comparison of parameters, which gives us the best results, meaning highest relaxation and lowest minimum yield.

Strain relaxation using Si^+ ion implantation is particularly desirable for high Ge content layers (25 at. %) where the relaxation process based on He^+ ion implantation and annealing suffers from certain limitations. Pseudomorphic 6 nm Si-cap/140 nm $Si_{0.71}Ge_{0.29}$ layers were processed using implantation parameters, which result in high relaxation and good layer quality for the $Si_{0.74}Ge_{0.26}$ layers. Consequently, in this case $D<0$ implantations were discarded. The main results are presented in Table III. The implantation fluence dependence is not significant at $D\sim0$, inducing about $R=80\%$. For deeper implants ($D>0$) the 29% Ge layers need only a dose of 8.5×10^{13} ions/cm^2 to get the highest degree of relaxation, while this dose gives only 34% relaxation in the 26% Ge layer. As previously presented, the 1×10^{14} ions/cm^2 implantation gives a similar result for 26% Ge. Layers with a lower Ge content of 20% require an even higher implantation dose of 1.5×10^{14} ions/cm^2. The data presented in Table III indicate that the dose necessary for an efficient relaxation process decreases with increasing Ge content in the alloy.

IV. DISCUSSION

In the following, we make an attempt to rationalize our central experimental result. Efficient strain relaxation of SiGe layers by Si^+ ion implantation combined with satisfactory strain transfer to Si-cap layers and good crystalline quality can be obtained only in a rather limited range of the relevant sample and implantation parameters. We first present a model of strain relaxation of SiGe layers below the amorphization limit and then discuss the effects of amorphization/recrystallization on strain relaxation, strain transfer, and sample quality.

A. Strain relaxation of SiGe layers below the amorphization limit

The most striking feature in Fig. 8 is the high sensitivity of the relaxation degree of SiGe layers to the Si implantation dose. Our basic assumption in modeling this sensitivity is that strain relaxation is due to the formation of dislocation loops acting as nuclei for strain relaxing MDs. This assumption is principally the same as for strain relaxation by He-ion implantation.[11] In the latter case, however, loops are emitted by highly pressurized cavities formed by the precipitation of the implanted He-atoms during annealing, whereas in the present case they result from the condensation of the excess SIAs corresponding to the number of Si ions implanted ("+1"-model[24]).

After annihilation of most of the Frenkel pairs associated with ion implantation, the remaining excess SIAs form small atomistic clusters, which grow by Ostwald ripening during annealing.[12,14] Clusters containing more than a few SIAs tend to form planar arrangements. Which type of planar arrangement is the energetically most favorable one depends on the size of the cluster as well as on the composition of the SiGe system.

The energetically most favorable small size planar cluster in pure Si (<20 nm) is a rodlike, dangling bond free arrangement of SIAs oriented along ⟨011⟩ directions on {311}-planes ({311}-defects).[12] At larger size (>20 nm) more compact (circular) dislocation loops are energetically more favorable. In the size range of 20–80 nm, faulted Frank partial loops with partial Burgers vector $\mathbf{b}=a\langle111\rangle/3$ perpendicular to their {111} habit planes have been observed. Above this size range, such faulted loops tend to transform by shear to perfect loops with $\mathbf{b}=a\langle110\rangle/2$ on the same {111} habit planes.[14] In SiGe, {311}-clusters occur only at low Ge content. For compositions between 20% and 30% Ge considered in the present work, only compact (circular) faulted (F) and perfect (P) loops have been observed depending on loop size.[15]

To our knowledge, the effect of high compressive plane stress in SiGe on the evolution of SIA clusters of dislocation loop type has not been analyzed so far. Under a planar compressive stress in SiGe, the fourfold energetic degeneracy of equivalent F loop variants is maintained, while the 12 fold degeneracy of equivalent P loops is removed; the energy of eight variants with **b** in the (001)-plane of the layers is increased, while that of the four variants with a component of **b** in [001]-direction is lowered. This implies that a plane stress in SiGe favors the evolution of P loops with $\mathbf{b}=a\langle011\rangle/2$, which are, in fact, the (only) ones contributing to strain relaxation.

In contrast to sessile F loops, P loops are able to glide along their glide cylinders and by this to lower their interaction energy in the field of the compressive plane stress of the SiGe layer. In fact, the stress field tends to turn the plane of P loops with $\mathbf{b}=a\langle011\rangle/2$ from a {111} plane toward a plane of maximum resolved shear stress, increasing by this the shear component and the size of the loop. The line tension represents a restoring force against this loop extending action of the stress field.

It is useful here to study the loop energetics in an infinite stress field as a function of the loop plane orientation. The detailed analysis for this limiting case, which will be presented elsewhere,[25] yields the following main result. When the actual loop size r of a loop related to the minimum size r_0 without inclination of the loop plane (determined by the

number of SIAs in the loop) exceeds a certain critical value r^*, the loop becomes unstable and starts to extend through the stressed material, shearing and strain relaxing it continuously. The critical loop size r^* is related to the line tension s of the loop and the plane stress σ according to

$$r > r^* \approx 1.32 r_0 \approx 1.16 s/(b|\sigma|), \tag{1a}$$

$$\text{with} \quad s \approx (\mu f b^2/4\pi)\ln(r^*/r_c) \quad \text{and} \quad \sigma = C\varepsilon. \tag{1b}$$

Here $\mu = 68$ GPa is the isotropic average of the elastic modulus, f is a factor of the order of one, accounting for the type of the dislocation, r_c is the effective core radius of the dislocations,[26] ε is the plane strain in the (001)SiGe layers, and $C=(C_{11}+2C_{12})(C_{11}-C_{12})/C_{11}=180$ GPa is the corresponding plane stress elastic modulus. In the realistic case of a SiGe layer of finite thickness, Eq. (1) represents a reasonable first order approximation for loop-surface distances large compared to the loop size.

A "supercritical" loop defined by $r > r^*$ extends through the SiGe layer to the SiGe/Si substrate and the SiGe/Si-cap interface or the surface, forming by this two TD segments connected by at least one MD segment in the SiGe/Si substrate, which extends by the stress driven motion of the two TD segments in opposite directions. It is useful here to estimate the critical loop size as a function of the strain/stress state in SiGe layer. Using Eq. (1a) in conjunction with Eq. (1b) we find for fully strained epitaxial SiGe layers with Ge content between 20% and 30% values of r^* between 7 and 5 nm, respectively. Relaxation of the strain by 70%–80% increases r^* to values between 30 and 20 nm, respectively. The loops with diameters $(2r)$ between 30 and 50 nm visible in Figs. 3 and 5(b) for a Ge content of 26% may thus be considered to be close to "criticality" after 77% relaxation.

Equation (1) represents only an energetic condition for an individual loop to participate in the strain relaxation process. The additional kinetic condition for a substantial contribution of Si implantation to strain relaxation is that a significant fraction of the loops evolving in the SiGe layer during annealing reaches the critical size before loop coarsening ends due to SIA diffusion and escapes to the surface.

Coarsening of SIA type dislocation loops in SiGe systems during annealing is due to conservative Ostwald ripening, i.e., the growth of large loops on the expense of small ones by emission and reabsorption of SIAs without significant SIA loss to the surface or into the interior. The condition for the realization of such a conservative coarsening process is that the mean diffusion length l_d between the emission and reabsorption of an emitted SIA is constrained to the width $W \sim R_p$ of the implanted Si ions, i.e., $l_d \ll W$. Using an appropriate relation between l_d and the mean loop size and density N of the SIA absorbing loops and requiring that $l_d \ll W$ is fulfilled before $r \to r^*$ is reached, we have derived a condition for the Si fluence I having the form[25]

$$I \gg r^*/(b^2 W) \approx r^*/(b^2 R_p). \tag{2}$$

According to Eq. (1) for the critical loop size r^*, the lower boundary for the Si fluence defined by Eq. (2) is inversely proportional to the stress in the SiGe layer and, consequently, to the Ge content in it. Using in Eq. (2) numerical constants appropriate for our implantation conditions, we indeed find minimum doses on the order of $10^{14}/\text{cm}^2$. Equation (2) predicts, however, a continuous decrease in the dose required for efficient strain relaxation with increasing width $W \sim R_p$ of the implantation profile, which is obviously in contrast to our experimental observation that the required dose even increases with R_p at large values of R_p. This apparent contradiction between model and experiment at large R_p is most likely due to the penetration of the implantation profile into the unstressed Si substrate where the above described model for stressed SiGe cannot be expected to be valid.

Differently from SIA clusters in the stressed SiGe layer, {311}-clusters as well as F and P loops develop in the Si substrate in the absence of stress. In the stress free Si, once formed P loops are not destabilized by stress as in the SiGe layer. The situation differs also substantially from the case of loop formation by He implantation into the Si substrate below the SiGe layer, where suitable P loops are favorably formed and driven to the Si/SiGe interface by the stress field of highly pressurized cavities.[11] In our case of Si implantation, only P loops forming within a narrow Si layer adjacent to the Si/SiGe interface of the order of the loop size may be considered to be attracted to the elastically softer SiGe layer. We think that, in fact, only a small fraction of the Si atoms implanted into the Si substrate is able to contribute to strain relaxation. This would explain why the Si dose required for efficient strain relaxation increases with increasing Si implantation range when the implantation range exceeds the width of the SiGe layer, i.e., when $D > 0$. This reasoning is also supported by the observation by Holländer *et al.*[17] that the deposition of a large fraction of the implanted Si in an underlying SiO_2 layer does not reduce the degree of relaxation of the SiGe layer.

Assuming consequently that only loops within the SiGe layer contribute to strain relaxation, we have constructed critical lines for efficient strain relaxation as a function of Si dose and Ge content as shown in Fig. 10. The dependence on the Ge content is due to the dependence of the critical loop size on the stress in the SiGe layer.

B. Effects of amorphization/recrystallization on strain relaxation, strain transfer, and layer quality

Unfortunately, for Si^+ ion implantation at room temperature with implantation energies in the chosen range, local amorphization occurs at roughly the same dose level (around 10^{14} ions/cm^2) required for significant strain relaxation by Si implantation induced dislocation loops. Fortunately, on the other hand, our experiments indicate that the somewhat different energy and dose dependences of the former and the latter processes leave some room in the parameter space for efficient strain relaxation of the SiGe layers combined with satisfactory strain transfer to the Si-cap layer and good sample quality by the latter process.

Information on the dependence of the critical dose for local amorphization on the implantation energy E is provided by SRIM simulations for the number of vacancies per depth increment and implanted Si^+ ion as a function of E and depth z denoted in the following as $\zeta_v(E,z)$ [see Fig. 1(b)]. The

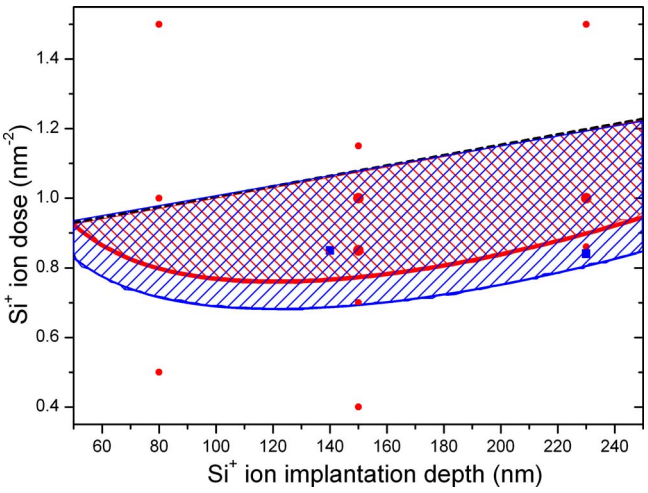

FIG. 10. (Color online) Critical lines separating regions of efficient/inefficient relaxation (full lines) in the ion dose/ion range representation for 150 nm thick $Si_{0.74}Ge_{0.26}$ layers (red thick line) and 140 nm thick $Si_{0.71}Ge_{0.29}$ layers (blue thin lines). The points represent our experimental results from Tables II and III. The dashed black line indicates the amorphization limits separating good/bad quality material. The region below the critical lines indicates samples with good quality but inefficient relaxation; the region above the critical lines and below the amorphization limits (cross-hatched) indicates good quality as well as efficient relaxation, and the region above the amorphization limits indicates efficient relaxation but bad quality.

local atomic vacancy concentration c_v for a given dose I is related to $\zeta_v(E,z)$ by

$$c_v(E,z) = I\zeta_v(E,z)\Omega, \tag{3}$$

where $\Omega \approx 0.02$ nm^3 is the (average) atomic volume of the material (Si or SiGe). Assuming that amorphization occurs when the vacancy concentration (Frenkel pair concentration) exceeds a certain critical value c_v^* and using Eq. (3), we can express the critical dose for local amorphization as

$$I^*(E,z) = c_v^*/[\zeta_v(E,z)\Omega]. \tag{4}$$

Since the maximum of $\zeta_v(E,z)$ decreases with increasing E [see Fig. 1(b)], the minimum critical dose $I^*(E)$ increases with increasing E. For 180 keV Si^+ implantation to a dose of $10^{14}/cm^2$, no indication of amorphization is found, whereas $1.5\times10^{14}/cm^2$ results in pronounced amorphization as demonstrated in Figs. 6 and 7(a). Hence, for 180 keV Si^+ implantation into 150 nm thick $Si_{74}Ge_{26}$, $I^*(180\ \text{keV})$ must have a value between these two doses. We assume here that $I^*(180\ \text{keV}) = 1.2\times10^{14}/cm^2$, which according to Eq. (3) with $\zeta_v(180\ \text{keV}) \approx 7.4$ per nm and ion corresponds to a critical vacancy concentration of $c_v^* \approx 18\%$. Using this in Eq. (4), we estimate with maximum values of $\zeta_v(E,z) \approx 9.2$ and 8.5 per nm and ion for the two other applied Si^+ implantation energies of 55 and 120 keV minimum values of $I^*(E)$ somewhat below and above $10^{14}/cm^2$ (9.8×10^{13} and $1.06\times10^{14}/cm^2$), respectively. These values are consistent with the doses above which the strain transfer efficiency and the quality of the samples worsen significantly as demonstrated by Table II and Fig. 8.

Within the limited accuracy of the SRIM simulations, the amorphization limit is approximately linear in the implantation range and, between 20% and 30% Ge, virtually independent of the Ge content. A linear fit to SRIM data is shown in Fig. 10 by the black dashed line.

TABLE IV. The relaxation degree and the width of the deconvoluted SiGe signals for 150 nm thick $Si_{0.74}Ge_{0.26}$ as a function of implanted Si^+ ion dose. The corresponding Raman spectra are presented in Fig. 9.

Implantation dose (ions/cm^2)	As-grown	8.5×10^{13}	1×10^{14}	1.5×10^{14}
SiGe relaxation degree (%)	0	35	78	82
SiGe Raman spectra width (cm^{-1})	4.8	5.2	5.5	7.2

The main question in the present discussion concerns the role of amorphization and recrystallization of SiGe layers for strain relaxation, strain transfer, and crystalline quality of the samples. We first consider a limiting case expected to occur at very high doses: complete and homogeneous amorphization of a top region of the sample from an amorphous/crystalline interface up to the surface. In this case, ideal epitaxial recrystallization would sweep out the whole damage including the excess SIAs associated with Si implantation through the surface; amorphization/recrystallization would not contribute to strain relaxation and strain transfer at all, and in the ideal case, the quality of the sample would be restored.

A qualitatively different case is local amorphization/recrystallization of a layer embedded into crystalline material (SiGe) at both sides. In this case, the system "remembers" the excess SIAs associated with Si implantation into the amorphous layer. Upon recrystallization of the amorphous layer from both sides, these SIAs must be incorporated into the restored crystal most likely in the form of dislocation loops. Such loops will contain all the excess SIAs associated with Si implantation into the amorphous layer—except part of these SIAs that were able to form one (or more) complete crystalline layer(s), which would, however, only occur well above the dose level applied in the present paper.

Accordingly, strain relaxation by amorphization/recrystallization induced by Si^+ ion implantation is also associated with dislocation loop formation as in the cases of Si^+ implantation into permanently crystalline material. There is, however, one important difference. The loops forming upon amorphization/recrystallization are expected to be concentrated in a narrow layer around the original location of the maximum vacancy concentration, to have irregular sizes, to be irregularly distributed, and to tend to entangle because of this. Consequently, the MD network resulting from their extension to the SiGe/Si substrate interface will be irregular and, therefore, will be associated with an inhomogeneous residual stress field in the SiGe layer after its partial relaxation. These arguments are confirmed by significant broadening of Raman peaks ($\Delta\omega_{SiGe}$) for the corresponding samples as seen in Table IV for the Raman spectra presented in Fig. 9. The loops visible in Figs. 3 and 5(b) may be considered to be caught in locally less well relaxed region where they are locally "critical" as discussed in conjunction with Eq. (1). Entangled dislocations in the SiGe/Si-cap interface

as seen in Fig. 3 hinder themselves from gliding to the surface, which results in a reduction in the strain transfer efficiency and the quality of the samples.

We may conclude that the occurrence of amorphization/recrystallization neither allows satisfactory strain transfer to Si-cap layers nor yields good quality of the samples and, therefore, should be avoided. To mark the parameter regions to be avoided we have included in Fig. 10 critical lines for local amorphization, in addition to critical lines separating regions of satisfactory and insufficient strain relaxation. As shown in Fig. 10, proper choice of implantation parameters allows efficient strain relaxation and strain transfer at good sample quality. Figure 10 indicates that the recommendable parameter range can be significantly widened by increasing the Ge content due to a decrease in the critical line for satisfactory strain relaxation at an insignificant decrease in the amorphization limit.

V. SUMMARY AND CONCLUSIONS

In this paper, we have presented a method for strain relaxation of SiGe layers based on Si^+ ion implantation and annealing. The most important result of our study is the efficient strain relaxation of the SiGe layer combined with efficient strain transfer to the Si-cap layer and a good crystalline quality of the layers can be obtained only in a narrow parameter window. A good example representing one point within this window is 120 keV Si^+ ion implantation to a dose of 8.5×10^{13} cm^{-2} into the range of the SiGe/Si interface of a 150 nm thick $Si_{0.74}Ge_{0.26}$ layer (followed by a 850 °C, 600 s anneal) for which 77% strain relaxation of the SiGe layer and 80% strain transfer to the Si-cap layer corresponding to a strain of 0.84% were obtained.

We have presented a summary of a model explaining our experimental findings in terms of dislocation loop formation of SIA type resulting from the clustering of excess SIAs associated with Si^+ ion implantation. To our knowledge, the evolution of such loops under the action of high compressive plane stress in SiGe is discussed here for the first time. Above a critical size, such loops spread unstably through the SiGe layer to its margins forming by this stress relaxing MD segments at the SiGe/Si substrate interface. The critical dose for the occurrence of this process is defined by the condition that the critical size of the loops is reached before loss of SIAs to the surface or into the sample interior terminates loop growth by conservative Ostwald ripening. It is shown that Si atoms implanted into the Si substrate do not significantly contribute to strain relaxation.

ACKNOWLEDGMENTS

The authors thank Dr. R. Carius's group (IEF-5, Forschungszentrum Juelich) for the Raman spectroscopy measurements, Dirk Rondas (IMEC) for his kindly assistance in the epitaxial growth, Mr. W. Michelsen for his assistance in the ion implantation, and Ms. Steffi Lenk for the TEM analysis.

[1] S. E. Thompson, M. Armstrong, C. Auth, S. Cea, R. Chau, G. Glass, T. Hoffman, J. Klaus, M. Zhiyong, B. McIntyre, A. Murthy, B. Obradovic, L. Shifren, S. Sivakumar, S. Tyagi, T. Ghani, K. Mistry, M. Bohr, and Y. El-Mansy, IEEE Electron Device Lett. **25**, 191 (2004).
[2] M. Reiche, C. Himcinschi, U. Gösele, S. Christiansen, S. Mantl, D. Buca, Q.T. Zhao, S. Feste, R. Loo, D. Nguyen, W. Buchholtz, A. M. Horstmann, D. Feijoo, and P. Storck, ECS Trans. **6**, 339 (2007).
[3] C. Mazure and A.-J. Auberton-Herve, Proceedings of the 31st European Solid-State Circuits Conference, 2005, ESSCIRC 2005, pp. 29–38.
[4] D. Greenlaw, G. Burbach, T. Feudel, F. Feustel, K. Frohberg, F. Graetsch, G. Grasshoff, C. Hartig, T. Heller, K. Hempel, M. Horstmann, P. Huebler, R. Kirsch, S. Kruegel, E. Langer, A. Pawlowitsch, H. Ruelke, H. Schuehrer, R. Stephan, A. Wei, T. Werner, K. Wieczorek, and M. Raab, Tech. Dig. – Int. Electron Devices Meet. **2003**, 277.
[5] T. Mizuno, N. Sugiyama, T. Tezuka, Y. Moriyama, S. Nakaharai, T. Maeda, and S. Tagaki, Tech. Dig. – Int. Electron Devices Meet. **2003**, 809.
[6] M. L. Lee, E. A. Fitzgerald, M. T. Bulsara, M. T. Currie, and A. Lochtefeld, J. Appl. Phys. **97**, 011101 (2005).
[7] J. Bogumilowicz, J. M. Hartmann, F. Laugier, G. Rolland, T. Billon, N. Cherkashin, and A. Claverie, J. Cryst. Growth **283**, 346 (2005).
[8] M. Luysberg, D. Kirch, H. Trinkaus, St. Lenk, S. Mantl, H.-J. Herzog, and T. Hackbarth, J. Appl. Phys. **92**, 4290 (2002).
[9] S. Mantl, D. Buca, B. Holländer, St. Lenk, N. Hueging, M. Luysberg, R. Carius, R. Loo, M. Caymax, H. Schäfer, I. Radu, M. Reiche, S. H. Christiansen, and U. Gösele, ECS Trans. **3**, 1047 (2006).
[10] D. Buca, B. Holländer, H. Trinkaus, S. Mantl, R. Carius, R. Loo, M. Caymax, and H. Schaefer, Appl. Phys. Lett. **85**, 2499 (2004).
[11] H. Trinkaus, B. Holländer, St. Rongen, S. Mantl, H.-J. Herzog, J. Kuchenbecker, and T. Hackbarth, Appl. Phys. Lett. **76**, 3552 (2000).
[12] D. J. Eaglesham, P. A. Stolk, H.-J. Gossmann, and J. M. Poate, Appl. Phys. Lett. **65**, 2305 (1994).
[13] B. Colombeau, N. E. Cowen, F. Cristiano, P. Calvo, N. Cherkashin, Y. Lamrani, and A. Claverie, Appl. Phys. Lett. **83**, 1953 (2003).
[14] F. Cristiano, J. Grisolia, B. Colombeau, M. Omri, B. de Mauduit, A. Claverie, L. F. Giles, and N. E. B. Cowern, J. Appl. Phys. **87**, 8420 (2000).
[15] R. T. Crosby, K. S. Jones, M. E. Law, A. Nylandsted Larsen, and J. Lundsgaard Hanses, Mater. Sci. Semicond. Process. **6**, 205 (2003).
[16] S. Boninelli, N. Cherkashin, A. Cleverie, and F. Cristiano, Nucl. Instrum. Methods Phys. Res. B **253**, 80 (2006).
[17] B. Holländer, D. Buca, M. Mörschbächer, St. Lenk, S. Mantl, H.-J. Herzog, Th. Hackbarth, R. Loo, M. Caymax, and P. F. P. Fichtner, J. Appl. Phys. **96**, 1745 (2004).
[18] J. F. Ziegler, J. P. Biersack, and U. Littmark, *The Stopping Range of Ions in Solids* (Pergamon, New York, 1985); SRIM, The Stopping and Range of Ions in Matter (http://www.srim.org/).
[19] L. C. Feldman, J. W. Mayer, and S. T. Picraux, *Materials Analysis by Ion Channeling* (Academic, New York, 1982).
[20] L. R. Doolittle, Nucl. Instrum. Methods Phys. Res. B **9**, 344 (1985).
[21] D. Buca, M. J. Mörschbächer, B. Holländer, M. Luysberg, R. Loo, M. Caymax, and S. Mantl, Mater. Res. Soc. Symp. Proc. **809**, B1.6.1 (2004).
[22] B. Doris, M. Ieong, H. Zhu, Y. Zhang, M. Steen, W. Natzle, S. Callegari, V. Narayanan, J. Cai, S. H. Ku, P. Jamison, Y. Li, Z. Ren, V. Ku, D. Boyd, T. Kanarsky, C. D'Emic, M. Newport, D. Dobuzinsky, S. Deshpande, J. Petrus, R. Jammy, and W. Haensch, Tech. Dig. – Int. Electron Devices Meet. **2003**, 631.
[23] J. Tsang, P. Mooney, F. Dacol, and J. Chu, J. Appl. Phys. **75**, 8098 (1994).
[24] M. D. Giles, J. Electrochem. Soc. **138**, 1160 (1991).
[25] H. Trinkaus, D. Buca, R. A. Minamisawa, and S. Mantl (unpublished).
[26] D. Hull and D. J. Bacon, *Introduction to Dislocation*, 4th ed. (Butterworth-Heinemann, Oxford, 2001).